Theoretical analysis of the photonic band structure of face-centred cubic colloidal crystals

1997 J. Phys.: Condens. Matter 9 10261

(http://iopscience.iop.org/0953-8984/9/46/023)

J. Phys.: Condens. Matter **9** (1997) 10261–10270. Printed in the UK PII: S0953-8984(97)84613-9

Theoretical analysis of the photonic band structure of face-centred cubic colloidal crystals

V Yannopapas†, N Stefanou† and A Modinos‡

† University of Athens, Section of Solid State Physics, Panepistimioupolis GR-157 84, Athens, Greece

‡ Department of Physics, National Technical University of Athens, Zografou Campus, GR-157 80 Athens, Greece

Received 30 May 1997, in final form 14 July 1997

Abstract. We present a theoretical analysis of the photonic band structure of fcc colloidal crystals in relation to experimentally available transmission spectra of finite slabs of such crystals.

1. Introduction

Photonic crystals with lattice spacings comparable to the wavelength of light have interesting properties and potentially many technological applications (see [1] for a recent review). Such crystals, which exhibit absolute frequency gaps in the optical region of the electromagnetic (EM) spectrum, are expected to have important applications in optoelectronics [2], but these may not be the only photonic crystals with interesting properties and applications. It has been shown, for example, that photonic crystals of appropriate structure may have an optical activity (turning the plane of polarization of incident light) much greater than that of naturally occurring optically active materials [3].

So far it has not been possible to fabricate a photonic crystal with an absolute frequency gap in the optical regime, but one by-product of this effort has been the experimental study of colloidal crystals with lattice spacings comparable to the wavelength of light [4, 5]. Under suitable conditions, a suspension of negatively charged polystyrene microspheres in water, interacting with a short-range repulsive Coulomb force and with a long-range attractive Van der Waals force, self-organize into an fcc crystal with a lattice constant which can be varied in a controlled manner at the preparation stage [6]. The photonic crystals obtained in this manner are worth studying, although they do not exhibit an absolute frequency gap because of the relatively low refractive index contrast between the microspheres and the surrounding medium. The colloidal crystals studied by Tarhan and Watson [4] were approximately 450 μm thick, consisting of about 1700 layers of (111) planes of polystyrene microspheres. The microspheres had a mean diameter of 0.135 μm monodisperse to within 4.2%, and occupied 5% of the total volume of the crystal. These crystals grow with the densest planes (111) parallel to the sample cell window, and in this way the [111] crystal direction is known *a priori*. The remaining information relating to the orientation of the crystal was obtained via a Kossel line analysis [4].

Tarhan and Watson [4] obtained transmission spectra over a wide range of wavelengths (475–800 nm) for light incident normally on the (111) surface of the above crystal, and for light incident at an angle, for both orthogonal components of the incident plane-polarized

0953-8984/97/4610261+10$19.50

beam. From these spectra they obtained approximate photon dispersion curves (frequency ω versus wavevector) for the given crystal. We shall discuss their data after we have introduced our theoretical results for the above quantities.

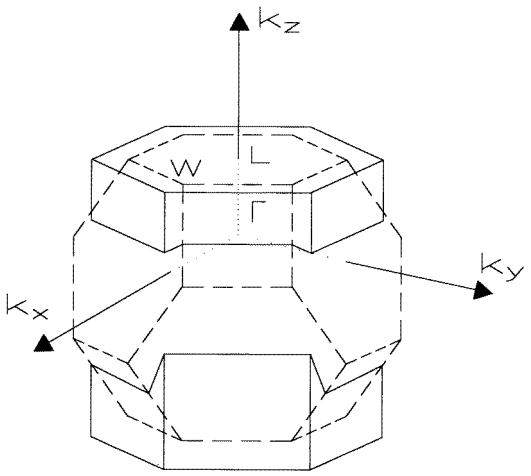

Figure 1. The reduced $\boldsymbol{k}$-zone associated with the (111) surface of an fcc lattice. The conventional first Brillouin zone is shown by broken lines.

2. Photon dispersion curves and transmission spectra of a colloidal crystal

We calculated the photon dispersion curves and the transmittance of the colloidal crystals discussed in [4] using the method that we have described in [7]. In all of our calculations concerning an infinite crystal, this is taken to be an fcc crystal with one polystyrene microsphere per lattice site. Each microsphere has a radius $R = 67.5$ nm, and a (relative) dielectric constant $\varepsilon_M = 2.59$. The medium (water) surrounding the microspheres has a dielectric constant $\varepsilon_w = 1.80$. The above values are exactly the same as those given in [4]. We have used for the lattice constant of the crystal the value $a = 465$ nm. This is somewhat smaller than the value $a = 469$ nm which was deduced in [4] from Bragg's law. We justify this by noting that, when $a = 465$ nm, the observed minimum in the transmittance through a slab of the material associated with Bragg reflection from the (111) planes (figure 3(a) of [4]) is accurately reproduced by our calculation. We point out that our method of calculation is exact and takes fully into account multiple scattering by the spheres. We note in passing that one obtains the same value for the lattice constant ($a = 465$ nm) by substituting in Bragg's law the observed position of the minimum in the transmittance and, instead of the dielectric constant of water which was used in [4], that (ε_{eff}) of an effective medium given by [8]

$$\frac{\varepsilon_{eff} - \varepsilon_w}{\varepsilon_{eff} + 2\varepsilon_w} = \beta \frac{\varepsilon_M - \varepsilon_w}{\varepsilon_M + 2\varepsilon_w} \tag{1}$$

where β is the volume fraction occupied by the microspheres.

Our method provides us with the complex-frequency band structure of the infinite crystal associated with a given crystallographic plane, and, in the present case, we have chosen this to be the (111) plane of the given fcc lattice. For given $\boldsymbol{k}_{\|}$, the component of the reduced

wavevector parallel to the (111) surface which lies in the surface Brillouin zone (SBZ) of the given surface (the outer hexagon formed by the solid lines in figure 1), we obtained the real-frequency lines, in the form

$$k_z = k_z(\omega; \boldsymbol{k}_\parallel). \tag{2}$$

A frequency line (2) gives the z-component of the wavevector (normal to the (111) surface) as a function of the frequency ω for given $\boldsymbol{k}_\parallel$, for the given line. The regions of ω over which k_z is real define corresponding frequency bands, and regions over which k_z is complex define corresponding frequency gaps (stop gaps). The corresponding solutions of Maxwell's equations (eigenfunctions of the EM field in the infinite crystal) are Bloch waves: the electric field component of the EM field (a similar equation is obeyed by the magnetic field) satisfies the equation

$$\boldsymbol{E}(\boldsymbol{r} + \boldsymbol{R}_n) = \mathrm{e}^{\mathrm{i}\boldsymbol{k}\cdot\boldsymbol{R}_n}\boldsymbol{E}(\boldsymbol{r}) \tag{3}$$

where $\boldsymbol{k} = (\boldsymbol{k}_\parallel, k_z(\omega; \boldsymbol{k}_\parallel))$. When k_z is real we have a propagating solution, and when k_z is complex we have an evanescent wave, which grows exponentially as $z \to +\infty$ or as $z \to -\infty$. In the infinite crystal, only propagating waves have a real existence. Using the periodicity of the band structure in the k_z-direction, i.e. $\omega(k_z + |\boldsymbol{b}^{(3)}|; \boldsymbol{k}_\parallel) = \omega(k_z; \boldsymbol{k}_\parallel)$, where $\boldsymbol{b}^{(3)} = (0, 0, 2\pi\sqrt{3}/a)$ is the primitive vector of the reciprocal lattice normal to the (111) plane, we define the reduced $\boldsymbol{k}$-zone appropriate to this surface as follows: $\boldsymbol{k} = (\boldsymbol{k}_\parallel, k_z)$, with $\boldsymbol{k}_\parallel$ in the SBZ and $-|\boldsymbol{b}^{(3)}|/2 \leqslant k_z < |\boldsymbol{b}^{(3)}|/2$. This is the hexagonal prism formed by the solid lines in figure 1. In the same figure we also show the conventional first Brillouin zone (BZ): the polyhedron formed by the broken lines. A propagating Bloch wave in the infinite crystal corresponding to a reduced wavevector within the BZ is obtained from one with a wavevector in the reduced $\boldsymbol{k}$-zone associated with the (111) surface, in the sense that a $\boldsymbol{k}$-point in the one zone has its equivalent point in the other: the two points differ by a vector of the three-dimensional reciprocal lattice if they do not coincide. Therefore, having calculated the real-frequency lines (2), we could obtain the dispersion curves along a symmetry line in the BZ to compare with the dispersion curves along the same line presented in [4]. It is worth noting that, when there is a plane of mirror symmetry parallel to the surface under consideration, as is the case with the (111) plane of the present fcc crystal, then, if there exists, for given ω, a Bloch wave with a reduced wavevector $\boldsymbol{k} = (\boldsymbol{k}_\parallel, k_z(\omega; \boldsymbol{k}_\parallel))$, there also exists a Bloch wave with reduced wavevector $\boldsymbol{k} = (\boldsymbol{k}_\parallel, -k_z(\omega; \boldsymbol{k}_\parallel))$ and, evidently, if one of these waves propagates (decays) to the right (in the positive z-direction) the other propagates (decays) to the left. The advantages to be had from a knowledge of the complex-frequency band structure are discussed in [7].

In figure 2(a), we show a real-frequency line for $k_\parallel = 0$ (the centre of the SBZ of the (111) surface), for ω in the region of the lowest frequency gap, associated with Bragg reflection from the (111) planes (in the figure we write, instead of ω, the corresponding wavelength of the incident light). The sections below and above the gap correspond to dispersion curves along the ΓL symmetry line of the BZ (figure 1). The real part of k_z over the frequency gap is constant and equals $|\boldsymbol{b}^{(3)}|/2$, the value at the edge of the reduced $\boldsymbol{k}$-zone defined in figure 1. The broken line in figure 2(a) gives $\mathrm{Im}\, k_z(\omega)$ over the gap; it essentially determines the attenuation of an EM wave in the infinite crystal and, therefore, the transmission coefficient of light incident normally on a slab of the material parallel to the (111) surface. We note that the bands shown in figure 2(a) are doubly degenerate, and that they couple, respectively, to the two orthogonal components of plane-polarized light, incident normally on the (111) surface.

The way to calculate the transmission coefficient is described in [7]. Using that method we calculated the transmission coefficient for light incident normally on a slab of the material

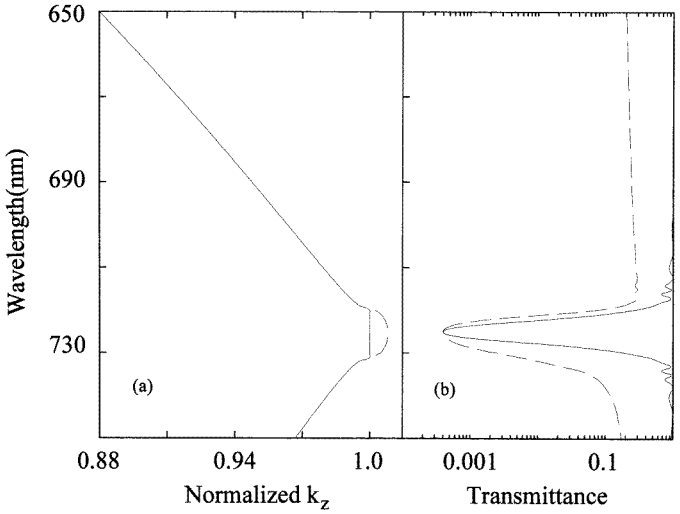

Figure 2. (a) The photonic complex band structure at the centre of the SBZ of a (111) surface of the given fcc colloidal crystal in the region of the lowest frequency gap. The dispersion curves are given over a limited region of the normalized z-component of the wavevector, $2k_z/|\boldsymbol{b}^{(3)}|$, near the edge of the reduced $\boldsymbol{k}$-zone. (b) The corresponding transmittance curve of a slab of 2^{11} layers parallel to the (111) surface. The solid (broken) line is obtained without (with) absorption taken into account.

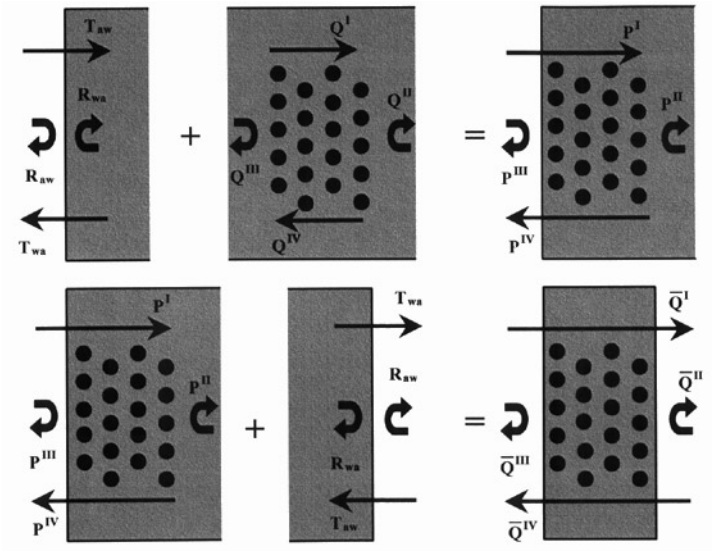

Figure 3. Schematic constructions of the reflection and transmission matrices for a colloidal crystal including the effect of the air–water interfaces.

2^{11} layers thick. The formulae given in [7] give the transmission and reflection matrices, denoted by Q in that paper, for light incident on a multilayer of spheres, assuming that the material surrounding the spheres in the crystal extends beyond the slab to infinity. In the present case the material surrounding the spheres in the slab is water and that on either

side of the slab is air with a dielectric constant $\varepsilon_a = 1.0$. Therefore light incident on either of the water–air interfaces, from either side, will be partly reflected at that interface. The way to take into account this scattering of the light at the interfaces is shown schematically in figure 3. One can easily show that the matrix elements $\bar{Q}$ for the reflection and the transmission of light incident on the slab from the left are given by

$$\begin{aligned} \bar{\mathbf{Q}}^{\mathrm{I}} &= \mathbf{T}_{wa}(\mathbf{I} - \mathbf{P}^{\mathrm{II}}\mathbf{R}_{wa})^{-1}\mathbf{P}^{\mathrm{I}} \\ \bar{\mathbf{Q}}^{\mathrm{III}} &= \mathbf{P}^{\mathrm{III}} + \mathbf{P}^{\mathrm{IV}}\mathbf{R}_{wa}(\mathbf{I} - \mathbf{P}^{\mathrm{II}}\mathbf{R}_{wa})^{-1}\mathbf{P}^{\mathrm{I}} \end{aligned} \tag{4a}$$

where

$$\begin{aligned} \mathbf{P}^{\mathrm{I}} &= \mathbf{Q}^{\mathrm{I}}(\mathbf{I} - \mathbf{R}_{wa}\mathbf{Q}^{\mathrm{III}})^{-1}\mathbf{T}_{aw} \\ \mathbf{P}^{\mathrm{II}} &= \mathbf{Q}^{\mathrm{II}} + \mathbf{Q}^{\mathrm{I}}\mathbf{R}_{wa}(\mathbf{I} - \mathbf{Q}^{\mathrm{III}}\mathbf{R}_{wa})^{-1}\mathbf{Q}^{\mathrm{IV}} \\ \mathbf{P}^{\mathrm{III}} &= \mathbf{R}_{aw} + \mathbf{T}_{wa}\mathbf{Q}^{\mathrm{III}}(\mathbf{I} - \mathbf{R}_{wa}\mathbf{Q}^{\mathrm{III}})^{-1}\mathbf{T}_{aw} \\ \mathbf{P}^{\mathrm{IV}} &= \mathbf{T}_{wa}(\mathbf{I} - \mathbf{Q}^{\mathrm{III}}\mathbf{R}_{wa})^{-1}\mathbf{Q}^{\mathrm{IV}}. \end{aligned} \tag{4b}$$

The reflection and transmission matrices for a flat interface between two different homogeneous media A and B (air (a) and/or water (w) in our case) are given by

$$\begin{aligned} [R_{AB}]_{gi;g'i'} &= \delta_{gg'}\begin{bmatrix} R_x\cos^2\phi + R_y\sin^2\phi & (R_x - R_y)\sin\phi\cos\phi & 0 \\ (R_x - R_y)\sin\phi\cos\phi & R_x\sin^2\phi + R_y\cos^2\phi & 0 \\ 0 & 0 & R_z \end{bmatrix} \\ [T_{AB}]_{gi;g'i'} &= \delta_{gg'}\begin{bmatrix} T_x\cos^2\phi + T_y\sin^2\phi & (T_x - T_y)\sin\phi\cos\phi & 0 \\ (T_x - T_y)\sin\phi\cos\phi & T_x\sin^2\phi + T_y\cos^2\phi & 0 \\ 0 & 0 & T_z \end{bmatrix} \end{aligned} \tag{4c}$$

where $i, i' = x, y, z$ and

$$\begin{aligned} &R_x = -\left[2\left(1 + \frac{\varepsilon_A k_z^B}{\varepsilon_B k_z^A}\right)^{-1} - 1\right] \qquad R_y = \left[2\left(1 + \frac{k_z^B}{k_z^A}\right)^{-1} - 1\right] \qquad R_z = -R_x \\ &T_x = 2\frac{\varepsilon_A k_z^B}{\varepsilon_B k_z^A}\left(1 + \frac{\varepsilon_A k_z^B}{\varepsilon_B k_z^A}\right)^{-1} \qquad T_y = 2\left(1 + \frac{k_z^B}{k_z^A}\right)^{-1} \qquad T_z = 2\frac{\varepsilon_A}{\varepsilon_B}\left(1 + \frac{\varepsilon_A k_z^B}{\varepsilon_B k_z^A}\right)^{-1} \\ &k_z^A = \sqrt{\frac{\omega^2}{c^2}\varepsilon_A - (\boldsymbol{k}_\parallel + \boldsymbol{g})^2} \qquad k_z^B = \sqrt{\frac{\omega^2}{c^2}\varepsilon_B - (\boldsymbol{k}_\parallel + \boldsymbol{g})^2}. \end{aligned} \tag{5}$$

In the above formulae the component of the wavevector parallel to the interface is written as $\boldsymbol{k}_\parallel + \boldsymbol{g}$, where $\boldsymbol{k}_\parallel$ is taken in the SBZ and $\boldsymbol{g}$ is the appropriate two-dimensional reciprocal-lattice vector [7]. We denote the azimuthal angle of $\boldsymbol{k}_\parallel + \boldsymbol{g}$ with respect to the coordinate system defined in figure 1 as ϕ. The incident and reflected waves are referred to an origin which is the midpoint between the first plane of the slab and the would-be preceding plane of the corresponding infinite crystal. The transmitted wave is referred to an origin at the midpoint between the last plane of the slab and the would-be next plane of the corresponding infinite crystal. The effect of the scattering at the interfaces on the transmittance is relatively small, but not negligible; it compares with the difference in the transmittance of the cell between the two incident polarizations.

All of the transmittance curves in the present work, unless otherwise stated, were calculated for a slab 2^{11} layers thick and with the scattering at the slab–air interfaces taken into account. We have also taken into account the small degree of absorption of light that does occur in the crystal by adding a small imaginary part $\mathrm{Im}\,\varepsilon_M = 0.01$ to the dielectric constant of the spheres. We can see that the transmittance shown in figure 2(b) is closely related to the corresponding real-frequency line shown in figure 2(a). In

the absence of absorption, the transmittance is practically unity over the allowed frequency bands, diminishing rapidly as the frequency moves from the edge to the centre of the frequency gap. Moreover, in the absence of absorption, the finite size of the slab introduces small oscillations in the transmittance at the band edges. When absorption is taken into account, these oscillations disappear and the transmittance is reduced at all frequencies, but not in a uniform manner: away from the resonance minimum the transmittance increases with the wavelength in agreement with the experimental observations [4].

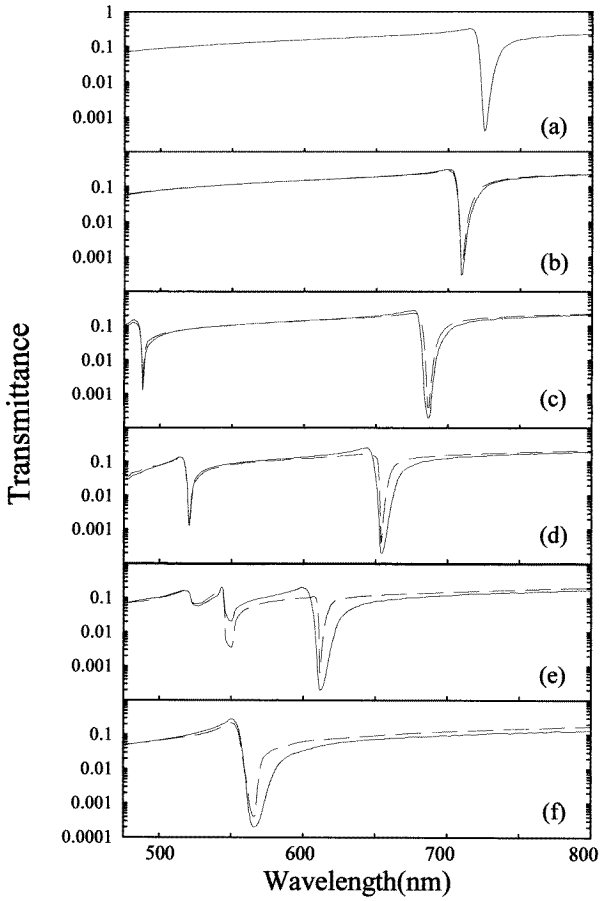

Figure 4. Transmittance curves for the given fcc colloidal crystal calculated for various angles of incidence. The solid (broken) lines refer to s (p) polarization of the incident light. (a) The L point, (b) L + 16°, (c) L + 26°, (d) L + 36°, (e) L + 47°, (f) the W point (L + 58°).

In figure 4 we present the results of our calculation for the transmittance of a slab for different angles of incidence. These transmittance curves are to be compared with the corresponding experimental curves (at the same angle of incidence) of Tarhan and Watson (figure 3 of [4]). The solid lines are obtained for s-polarized incident light: this is called vertical polarization in [4]; the electric field component of the incident light is parallel to the surface of the slab and oscillates along the y-direction (i.e. normal to LW). The dashed lines are obtained for p-polarized incident light: this is called horizontal polarization in [4]; the electric field component of the incident light lies in the plane of incidence (the

xz-plane). The agreement between theory and experiment is on the whole quite good. The variation with angle of the higher-wavelength minimum in the transmittance (due basically to a frequency gap generated by Bragg reflection from the (111) planes) is reproduced very well by the calculation; the shape of the transmittance curve about this minimum, its dependence on the polarization of the incident light, and the variation of these quantities with angle are reproduced reasonably well but not exactly by our calculation. The second minimum in the transmittance curve appearing when the angle of incidence equals 26°, which is associated with Bragg reflection from the (002) planes, is also reproduced by the calculation (figure 4(c)), but its calculated shape, especially when the angle of incidence is 47° (figure 4(e)), appears more complicated than its observed shape. We suspect that this might be due to deviations from the perfect periodicity (all spheres have the same radius and are arranged perfectly periodically in space) which we have assumed in the calculation. Moreover, a third weak minimum, associated with Bragg reflection from the $(\bar{1}11)$ planes, appears at a lower wavelength when the angle of incidence is 47° (figure 4(e)). We note that the dependence of the transmittance on the polarization of the incident light exists at all angles (except at normal incidence (figure 4(a))) as in the experiment. Finally, we note that a small minimum in the transmittance curves observed experimentally at $\lambda \cong 475$ nm, for angles of incidence 47° and 51.1°, is not reproduced by the corresponding calculations.

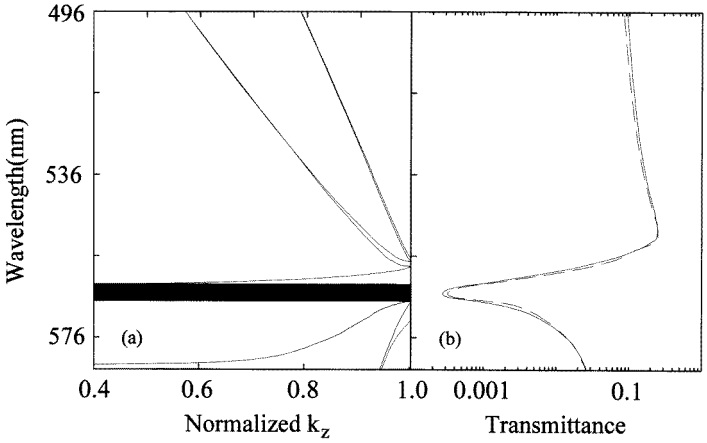

Figure 5. (a) The photonic band structure, for $\boldsymbol{k}_{\parallel} = (\sqrt{2}\pi/a, 0)$, in the region of the lowest frequency gap. The dispersion curves are given over a limited region of the normalized z-component of the wavevector, $2k_z/|\boldsymbol{b}^{(3)}|$, near the edge of the reduced $\boldsymbol{k}$-zone. The shaded region representing the gap for the given $\boldsymbol{k}_{\parallel}$ extends to $k_z = 0$. (b) The corresponding transmittance curve of a slab 2^{11} layers thick parallel to the (111) surface, for light incident with the same $\boldsymbol{k}_{\parallel}$. The solid (broken) line refers to s- (p-) polarized incident light.

We shall next discuss the possibility of obtaining from the transmission curves (such as those of figure 4) the width of the frequency gap as a function of $\boldsymbol{k}_{\parallel}$ which is determined, of course, by the angle of incidence for a given frequency. We have already shown in figure 2(a) the frequency bands, near the frequency gap, corresponding to $\boldsymbol{k}_{\parallel} = 0$, which determine the transmittance, shown in figure 2(b), for normal incidence on a (111) slab of the crystal. In figure 5(a) we show the frequency bands in the vicinity of the frequency gap (the dispersion curves are given for k_z near the edge of the reduced $\boldsymbol{k}$-zone), for $\boldsymbol{k}_{\parallel} = (k_x, k_y) = (\sqrt{2}\pi/a, 0)$ which coincides with the projection of the W point on the

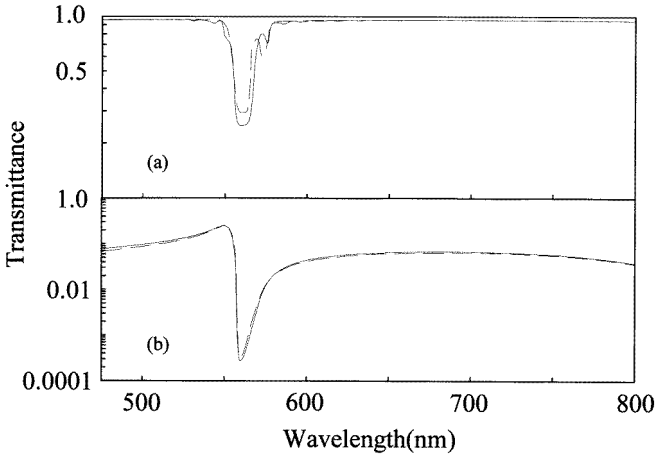

Figure 6. Transmittance curves for $\boldsymbol{k}_{\parallel} = (\sqrt{2}\pi/a, 0)$. (a) For a slab 2^5 layers thick. (b) For a slab 2^{11} layers thick. The solid (broken) lines refer to s- (p-) polarized incident light.

SBZ of the (111) surface (see figure 1). For the above $\boldsymbol{k}_{\parallel}$, the edge point coincides with the W point of the conventional BZ. At the W point we have three doubly degenerate eigenfrequencies (the corresponding eigenmodes have the W_3 symmetry), and two non-degenerate eigenfrequencies, the lower of which corresponds to an eigenmode of symmetry W_2' with the higher one corresponding to an eigenmode of symmetry W_1. Away from the W point, the degeneracy is lifted and one obtains eight non-degenerate frequency bands. We note that the frequency gap appears between two doubly degenerate bands (at the W point) and that the partners in each band couple respectively to the two different polarizations of the incident radiation. We therefore expect that the transmittance of light through a thick slab of the crystal will be practically independent of the polarization, when the frequency of the incident light lies within the gap and its direction of incidence is such that the $\boldsymbol{k}_{\parallel}$-component of the wavevector coincides with the projection of the W point on the SBZ. The above implies that the attenuation of the incident light is determined by the imaginary component of k_z of the real-frequency lines associated with the above-mentioned degenerate bands, and it will be true of course only for sufficiently thick slabs. This is demonstrated in figure 6, which shows the transmittances of a 2^5-layers-thick slab and a 2^{11}-layers-thick slab. We can see that the transmittances for the two different polarizations are practically the same only for the thick slab, for which it is appropriate to use the eigenmodes of the infinite crystal in analysing the data.

It is important to note that the frequency gap for given $\boldsymbol{k}_{\parallel}$ is determined *by the projection* of the corresponding frequency lines (2) on the SBZ as shown in figure 5 for a particular $\boldsymbol{k}_{\parallel}$, and not by the eigenfrequencies at the edge of the reduced $\boldsymbol{k}$-zone. The shaded region in figure 5, representing the gap for $\boldsymbol{k}_{\parallel} = (\sqrt{2}\pi/a, 0)$, extends to $k_z = 0$. We could in the same manner obtain the real-frequency lines for any $\boldsymbol{k}_{\parallel}$ in the SBZ, and the corresponding frequency gap if indeed one such existed for that $\boldsymbol{k}_{\parallel}$. We have chosen instead, in order to compare with the experimental results [4], to calculate the eigenfrequencies for every $\boldsymbol{k}$ on the LW line (see figure 1). Our results are shown by the solid lines in figure 7. It is evident from this figure that the calculated eigenfrequencies converge at the point W, which implies, of course, that no absolute frequency gap exists.

A transmission experiment can, at best, determine the eigenfrequencies which define,

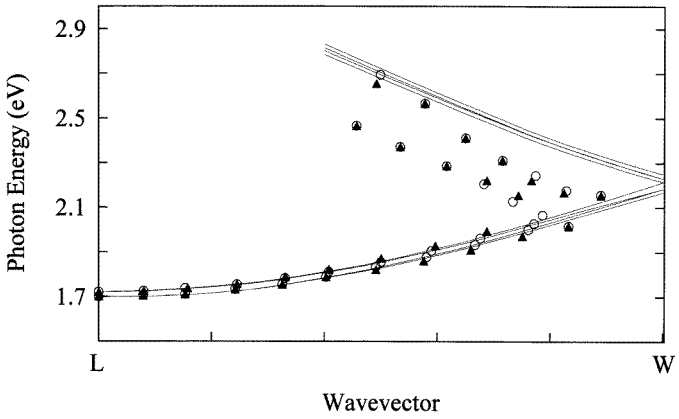

Figure 7. The photonic band structure along the LW line. The solid lines are calculated dispersion curves. The circles (corresponding to p-polarized incident light) and the triangles (corresponding to s-polarized incident light) have been obtained from experimental transmission data [4].

respectively, the upper and lower edges of a frequency gap and not all eigenfrequencies at a given $\boldsymbol{k}_{\parallel}$. Tarhan and Watson [4] identify the lower and upper limits of a frequency gap for a given angle of incidence and not for a given $\boldsymbol{k}_{\parallel}$. They identify these limits with those frequencies below and above the minimum of the normalized transmittance, respectively, where this transmittance equals 10^{-2}, for the given angle of incidence. However, the calculated transmittance curves show that as the imaginary component of k_z increases quite slowly away from the edge of the forbidden band, there is a large amount of arbitrariness in the positions of the band edges determined in this manner, dependent on the choice of transmission factor picked as representing the band edge. We note, moreover, that the $\boldsymbol{k}_{\parallel}$-component of the lower limit of the gap defined in the manner of Tarhan and Watson [4] is not the same as the $\boldsymbol{k}_{\parallel}$-component of the upper limit. The above authors wrongly identify the limits of the gaps defined in this manner with the eigenfrequencies on the LW line. It is also worth noting that away from the L and W points, a band does not couple exclusively with s- or p-polarized light but to a varying degree with either of them. In order to clarify the above we show in figure 7 the limits of the 'gaps' (circles and triangles) corresponding to the two transmission minima of figure 3 of [4], but as a function of $\boldsymbol{k}_{\parallel}$, rather than the angle of incidence. We can see that in general these limits do not correspond to the eigenfrequencies for $\boldsymbol{k}$ along the LW line, as expected from our arguments above.

3. Conclusion

We may conclude that for a proper analysis of the experimental data, one has to calculate the transmittance for a given slab of the colloidal crystal and compare directly with the corresponding data, and if these agree, one can with confidence accept the theoretical dispersion curves which underlie the calculation of the transmission spectra. But an estimate of these dispersion curves directly from the experimental data in the manner of Tarhan and Watson [4] is limited in its scope by the factors discussed in the previous section.

References

[1] Soukoulis C M (ed) 1996 *Photonic Band Gap Materials* (Dordrecht: Kluwer)
[2] Yablonovitch E 1993 *J. Phys.: Condens. Matter* **5** 2443
[3] Karathanos V, Stefanou N and Modinos A 1995 *J. Mod. Opt.* **42** 619
[4] Tarhan I I and Watson G H 1996 *Phys. Rev. Lett.* **76** 315
[5] Vos W L, Sprik R, van Blaaderen A, Imhof A, Lagendijk A and Wegdam G H 1996 *Phys. Rev.* B **53** 16 231
[6] Pieranski P 1983 *Contemp. Phys.* **24** 25
[7] Stefanou N, Karathanos V and Modinos A 1992 *J. Phys.: Condens. Matter* **4** 7389
[8] Abèles F, Borenzstein Y and Lopez-Rios T 1984 *Festkörperprobleme (Advances in Solid State Physics)* vol 24 (Braunschweig: Vieweg) p 93